

Journal Pre-proof

Characterization of groundwater –surface water interactions using high resolution integrated 3D hydrological model in semiarid urban watershed of Niamey, Niger

Abdou Boko Boubacar, Konaté Moussa, Nicaise Yalo, StevenJ. Berg, Andre R. Erler, Hyoun-Tae Hwang, Omar Khader, Edward A. Sudicky



PII: S1464-343X(19)30394-2

DOI: <https://doi.org/10.1016/j.jafrearsci.2019.103739>

Reference: AES 103739

To appear in: *Journal of African Earth Sciences*

Received Date: 10 May 2019

Revised Date: 25 October 2019

Accepted Date: 13 December 2019

Please cite this article as: Boubacar, A.B., Moussa, Konaté., Yalo, N., Berg, S., Erler, A.R., Hwang, H.-T., Khader, O., Sudicky, E.A., Characterization of groundwater –surface water interactions using high resolution integrated 3D hydrological model in semiarid urban watershed of Niamey, Niger, *Journal of African Earth Sciences* (2020), doi: <https://doi.org/10.1016/j.jafrearsci.2019.103739>.

This is a PDF file of an article that has undergone enhancements after acceptance, such as the addition of a cover page and metadata, and formatting for readability, but it is not yet the definitive version of record. This version will undergo additional copyediting, typesetting and review before it is published in its final form, but we are providing this version to give early visibility of the article. Please note that, during the production process, errors may be discovered which could affect the content, and all legal disclaimers that apply to the journal pertain.

© 2019 Published by Elsevier Ltd.

29 **Abstract**

30 This study investigates groundwater-surface water interactions using an equivalent porous
31 medium approach in a data scarce and semi-arid hydrogeological watershed located south-
32 west Niger. A large scale fully-integrated hydrologic model was built and calibrated using
33 HydroGeoSphere with a sequential approach of increasing levels of temporal resolution: 1)
34 steady state average conditions; 2) dynamic equilibrium with repeating monthly normal
35 forcing data; and 3) fully transient conditions. This approach provided a useful and
36 straightforward method for reducing the calibration effort of the large-scale fully-integrated
37 hydrologic model. River-aquifer exchange flux dynamics, water balance components for
38 different land use classes, as well as basin average groundwater recharge were computed from
39 the model. Simulation results show that exchange flux between groundwater and surface
40 water are important processes in the basin, with the Niger River acting primarily as a gaining
41 stream, with local losing zones. Ephemeral streams constitute important focused groundwater
42 recharge areas, while ponds exhibit either groundwater discharge behavior, or a recharge zone
43 profile depending on local topography. The basin average water balance highlights the
44 importance of plant transpiration (58 % of total rainfall) over surface evaporation (8%), with
45 groundwater recharge of up to 5% of total rainfall. Overland flow and infiltration account for
46 11% and 16 % of the total annual rainfall respectively, and groundwater discharge to the river
47 is 2% of the total rainfall

48

49

50

51 **Introduction**

52 The Niger River watershed covers approximately 7% of the surface area of Africa and is the
53 major source of agriculture related socio-economic activities for more than 100 million people
54 across nine countries (Benin, Burkina Faso, Cameroon, Chad, Côte d'Ivoire, Guinea, Mali,
55 Niger and Nigeria). The Niamey watershed considered in this study has an area of
56 approximately 1900 km² and is centrally located within the Niger River basin (Figure 1a and
57 Figures 1b). Furthermore, the Niger River is of crucial importance in the Niamey watershed,
58 as it constitutes the only permanent source of agricultural and domestic water needs.

59 It has been extensively reported that agro-pastoral production in the region is heavily affected
60 by the interannual variability of rainfall over different spatio-temporal scales (Tarhule and
61 Lamb 2003; Lebel et al., 1997; Lebel and Ali2009; Dai et al., 2004; Mahé et al., 2009). The
62 natural variability associated with several rainfall indices between 1940 and 2010 reflect a
63 high level of population vulnerability with 85% of activities linked to rain fed agriculture.
64 This vulnerability is enhanced by rapid population growth resulting in increasing water
65 demand.

66 To date studies have focused on rainfall variability, the Niger River flows rainfall
67 characteristics and climate change, groundwater recharge and quality(Anderson et al., 2017;
68 Leduc et al., 2001; Favreau et al., 2009; Girard, 1993; Williams, 1993, Ibrahim et al.,
69 2014;Hassane et al., 2017; Mascaro et al., 2015).However, presently no studies exist for the
70 Niger River Basin (or sub-basins) which explicitly consider the dynamics of groundwater and
71 surface water interaction in a fully-integrated manner.

72 Sustainable river basin management is one of the most prudent adaptation strategies to
73 climate variability and change, and to respond to increasing demand for agricultural and
74 resource development water in the Niger River basin. Providing scientifically-based
75 management policy to water resources managers requires properly addressing the
76 hydrological risks from natural and anthropogenic stresses on water resources and should rely
77 on integrated management at watershed scale (Berg and Sudicky, 2019). Therefore, delivering
78 information on hydrologic system responses to increasing extreme events (floods, drought)
79 frequency in the watershed requires the understanding of integrated hydrological processes at
80 the large watershed scale. The challenges of scarce data, complex surface-subsurface
81 interactions, as well as the high computational demand associated with integrated models is

82 probably one reason why relatively few publications on the application of fully integrated
83 models at the large scale exist in the literature (Barthel and Banzhaf ,2016). Although, it is
84 widely acknowledged that integrated surface-subsurface models are useful for water resources
85 managers, the application of these models would also be useful in order to support resources
86 development and sustainable water management in the Niger River basin. In the Niamey
87 watershed, most of the water for Niamey city and surrounding villages is supplied by treated
88 water from the Niger River, which is the only permanent river in the basin. The main
89 tributaries of the Niger River in Niamey are ephemeral streams, called koris. The groundwater
90 in the Continental Terminal sandstone formation, and the fractured aquifers of the
91 Precambrian basement, cover the remaining water demand of the watershed. Studies carried
92 out in the watershed have shown that groundwater recharge in the Continental Terminal
93 aquifer is predominantly governed by depression focused recharge (Desconnets et al.,1997;
94 Favreau et al., 2012,) through ponds, with less contribution from diffuse recharge (Ibrahim et
95 al.,2014) depending on land use types. Girard et al, (1997) has shown that the main recharge
96 process in fractured aquifers is controlled by the fracture system. The aforementioned existing
97 studies either investigated recharge using traditional water level fluctuation methods
98 combined with hydrochemicals and isotopes approaches, or groundwater models with loosely
99 coupled or simple representation of surface water, and vice versa.

100 Because the application of fully integrated hydrological models to large scale watersheds is a
101 growing area of the literature, only a few manuscripts have been published that provide
102 methodologies or guidance on the application of large scale integrated groundwater surface
103 water models (i.e., Erler et al., 2019; Barthel and Banzhaf , 2016, Hwanget al.,2018; Hwang et
104 al.,2015; Chen et al.). Additionally, to the author's knowledge, fully coupled surface-
105 subsurface models have not yet been applied for the whole of the Niger River basin or its sub-
106 basins. Moreover, none of the previous studies quantified directly the relation between Niger
107 River and the underlying aquifer systems.

108 Therefore, for resilient water resources management in the context of increasing demand
109 (irrigation and livestock, demography), along with variability and climate change,
110 characterization of the interactions between the Niger River drainage system, and underlying
111 aquifers is necessary. Furthermore, understanding and quantifying the interactions between
112 the river drainage system and aquifers is very important for alleviating the impact of recurrent
113 extreme events as it can provide valuable guidance for water resources management policies
114 in the watershed. For instance, determining flux exchange direction and magnitude between

115 the river and underlying aquifers can help support minimum environmental flows of the river
116 or buffer flood events (loosing river). The groundwater table may also act as a flood amplifier
117 in case the river or part of its reach is gaining. Understanding the groundwater surface water
118 interaction will also provide useful information for groundwater management purposes.
119 Characterization of this type of groundwater surface water interactions is very complex in
120 general, and particularly challenging in data scarce and semi-arid watersheds.

121 The first objective of this paper is to provide methodological guidance in the development of
122 watershed scale integrated surface-subsurface models in data scarce and semi-arid
123 environments. The second objective is to determine the magnitude and direction of the
124 exchange of water between the surface water system and complex groundwater aquifer
125 systems. The third objective is to provide practical information to water managers on the
126 water balance components considering different land use types, groundwater systems, as well
127 as surface water bodies.

128 **2. Data and Methods**

129 **2.1 Study area**

130 The study area corresponds to the Niamey watershed located south west of Niger (Figure 1b)
131 and the hydrogeological watershed considered in this study covers 1900 km². It is a semi
132 urban watershed with a population of 1.3 million. The rainfall patterns are characteristic of the
133 semi-arid climate with a dry season from October to May, and a rainy season from June to
134 September. Precipitation is dominated by heavy rainfall events with low frequency, typical of
135 the West African summer monsoon rainfall. The mean annual rainfall from 1947 to 2007 is 560
136 mm, and the mean annual Penman Monteith potential evapotranspiration is 2500 mm with an
137 average temperature of 29°C.

138 Recent land use maps (CILSS, 2016) indicate that agricultural land covers 11 % of the
139 watershed, natural vegetation of Sahelian savanna and steppe cover 32% and bare and sandy
140 soil cover 45% of the watershed. The main city and surrounding village occupy
141 approximately 8 %, and water bodies cover the remaining are 4 %.

142 *2.1.1. Geology and Hydrology of Niamey watershed*

143 According to its geographical position, the Niamey watershed is located on the western edge
144 of the Paleoproterozoic basement of the Liptako, and on the southeastern part of the

145 Iullemeden sedimentary basin. The Niamey watershed terrains consist of two main
146 geological units, including:

- 147 - The Paleoproterozoic basement (2300-2000 Ma ((Soumaila et Konaté, 2005), which
148 outcrops to the west of the study area at the vicinity of the Niger River. It includes
149 granitoid plutons alternating with Greenstone belts. Granitoids consist of diorite
150 intrusions, quartz diorite to tonalite, monzonite, granodiorite and granite or syenite
151 locally. These intrusive bodies are either syn-tectonic or post-tectonic (Machens,
152 1973; Soumaila et Konaté, 2005; Perotti et al., 2016). The greenstone belts consist of
153 sandstones-pelitic rocks more or less metamorphosed (shales, sericite schists,
154 micaceous schists, quartzitic schists) and low to medium metamorphic greenstone
155 (amphibolite, chlorite schists, metabasalts, metagabbros) (Machens, 1973; Soumaila et
156 Konaté, 2005; Perotti et al., 2016).
- 157 - The sedimentary deposits overlie unconformably the Paleoproterozoic basement. The
158 lowermost deposits are represented by an older unit essentially consisting of Upper
159 Precambrian sediments (Niamey sandstone) (Machens, 1973) and the uppermost
160 deposits consist of the clayish to silty sandstones of the Oligocene Continental
161 Terminal 3 formation (CT3) (Chardon et al., 2018) and quaternary to recent deposits
162 that infill the ephemeral streams and the Niger River.

163

164 The hydrogeology of the watershed is characterized by the geological conditions, with two
165 types of aquifers. The fractured aquifers of the Liptako basement formations are found in both
166 the granitic and Greenstone belts formations, and the Continental Terminal, CT3 aquifer
167 (Figure 2a). Depth to groundwater table varies from 5 m in the fractured aquifers, to 50 m in
168 the CT3 aquifer.

169 The hydrological conditions of the watershed are quite complex. The only permanent
170 freshwater source is the Niger River, and its flow is generated from the upper Niger basin in
171 the Fouta Djallon Massif in Guinea. In the study area, the Niger River flow has two peaks,
172 one peak due to the contribution of the local rainy season in September and the other in
173 December due to the inflow from upstream (Andersen et al., 2005). The other hydrological
174 features are the endorheic ephemeral stream, called koris that are hydrologically active during
175 the rainy season, and surface runoff discharge into a mosaic of permanent and semi
176 permanent ponds where groundwater recharge is shown to occur (Massuel et al. 2011). The
177 strong spatial variability of the ephemeral stream and the ponds drainage area is critical to the

178 determination of watershed area, due to the general endorheic configuration of the landscape
179 .Therefore, to summarize the complex hydrological setting, the Niger River flow is driven by
180 the inflow coming from upstream, and the local precipitation that drives ephemeral stream
181 and ponds.

182 **2.2. Data set**

183 *2.2.1 Geological data*

184 A 3D geological model of the watershed is built (Figure 2b) using Machens' (1973)
185 geological map and more than 120 borehole logs documented by Bernert et al.(1985) and
186 Dehays et al.(1986). The construction of the 3D geological model of the study area involves
187 the lithological interpretation of the individual 120 borehole logs to create 2D surface maps of
188 model layers. The interpolation was performed using the inverse distance weighting method.
189 Based on different lithological elevations of the boreholes, a grid model and contour map of
190 geological layers were built. Then, from the grid model and contour map of the different
191 geological layers, a 3D geological model was constructed, as defined in the HGS grok
192 command file.

193 The inverse-distance method represents one of the more common gridding methods. In this
194 method, the value assigned to a grid node (cell value) is a weighted average of either all of the
195 data points or a number of directionally distributed neighbors. In this case, the cell values
196 represent the absolute elevation of the interfaces between lithological formations, which have
197 been derived from the boreholes.

198 The fractured aquifer is characterized by three different units: The granitic formations are
199 intrusive into the birrimian greenstone belt formation. However, this geological configuration
200 was simplified in the 3D geological model by considering the granitic aquifer at the bottom of
201 the model and the greenstones belts formations aquifer at the top of the granitic layer. The
202 third aquifer is composed of weathered formations, consisting up to the undifferentiated
203 weathering horizons of both granite and schist formations.

204

205 Six geological units are included in the geological model; from bottom (oldest) to top
206 (youngest): the granitic formation of the Precambrian basement, the birrimian Greenstone
207 belts formations, the undifferentiated weathering zone of basement formations, and the

208 Continental Terminal CT3 formations. The CT3 formation is subdivided in its three
209 geological facies of clay, clayish sandstones, and silty sand. Hydraulic conductivities and
210 specific storage values for each geological unit are derived from literature. Initial estimates of
211 hydraulic conductivities for the fractured aquifers are taken from Domenico and Schwartz
212 (1990), while CT3 hydraulic conductivity was from (Favreau 2000). Manual parameter
213 estimation is performed during the calibration process and this is the first estimation of
214 hydraulic conductivities and Van Genuchten parameters of the fractured aquifer at regional
215 scale (Table 2).

216

217 *2.2.2. Soil and Land Use data*

218 Soil data used in this study are derived from Graef et al., (1998), who used soil types,
219 geomorphologic and hydrological criteria to extensively map the soil and terrain in south west
220 Niger, and provide a complete Soil and Terrain Digital Database(SOTER). The study area is
221 discretized in 41 soil zones derived from the SOTER database. Unsaturated soil zone K
222 values, porosity and Van Genuchten (1980) soil hydraulics parameters for the 41 SORTER
223 based soil zones are estimated by grain-size derived estimates using the ROSETTA neural
224 network prediction method (Schaap et al. 2001). Pressure saturation curves for the 41 soil
225 zones were derived from the Van Genuchten soil hydraulic parameters.

226 2013 land use map (CILSS, 2016) at 2km resolution was reclassified at 30m resolution into
227 six different classes consisting of Sahelian short grass savanna, steppe, agriculture, water
228 bodies, rocky and sandy land, and settlements. Leaf Area Index for the agriculture land use
229 class was determined from Levy and Jarvis (1999), and for the natural vegetation from Iio and
230 Ito (2014).

231 *2.2.3 Hydroclimate forcing data*

232 Hourly climate data for rainfall, maximum and minimum temperatures (T_{max} , T_{min}), wind
233 speed, relative humidity and solar radiation from 2011 to 2017 were obtained from an
234 automatic weather station installed at the Agriculture Hydrologie et Meteorologie
235 (AGRHYMET) Regional Center. Daily Penman-Monteith potential evapotranspiration was
236 computed using aggregated hourly data from the above weather station.

237 Stream flow gauging stations of Kandadji and Niamey were used in the model along the
238 Niger River part of the modeled watershed. Kandadji gauge represents the closest upstream
239 gauging location and is used to define inflow to the upstream end of the model domain. The

240 gauging station (Fig 1b) located in the middle of the watershed is used to calibrate the
 241 integrated hydrological model. Daily time series for both gauging locations were obtained
 242 from the Niger Basin Authority (NBA) database.

243 A total of 24 observation wells were selected to calibrate the models for hydraulic heads
 244 based on the availability and aquifer types screened. 8 observation wells out of the 24 are
 245 piezometers equipped with automatic pressure recorder and are installed in the fractured
 246 aquifer and groundwater heads were recorded hourly from 2014 to 2017. The rest of
 247 observation wells are open wells with large diameter (1m), and/or boreholes pumped mostly
 248 to supply water for domestic use, whose pumping rate is as small as 1m³/day (Hassane, 2016).
 249 Hydraulic head data for all the observation wells was provided by the Direction Régional de
 250 l'Hydraulique et de l'Assainissement de Niamey and the NBA.

251 **2.3. Hydrological Model**

252 A 3D fully-integrated surface and subsurface hydrologic model, HydroGeoSphere (HGS)
 253 (Aquanty Inc, 2017) was used to calculate overland flow, variably-saturated groundwater
 254 flow, flux exchange between the Niger river, ephemeral stream, ponds and the aquifer system
 255 (i.e., CT3 and the fractured aquifer). Also water balance components such as groundwater
 256 infiltration/exfiltration and evapotranspiration for various land use types were computed.
 257 HGS uses control-volume finite element/difference method to implicitly solve a modified
 258 form of Richards' equation for 3D variably-saturated subsurface flow and a depth-integrated
 259 Saint Venant diffusion wave equation for 2D surface water flow in a parallelized manner
 260 (Hwang et al., 2014) as described in Equation (1).

$$261 \quad \nabla \cdot (k_r \mathbf{K} \nabla h) \pm Q + \Gamma = \frac{\partial}{\partial t} (\theta_s S_w) \quad (1)$$

262 where k_r is the relative permeability, representing the water saturation function S_w or the
 263 pressure head ψ , \mathbf{K} is the hydraulic conductivity tensor, h corresponds to the total head
 264 provided by $\psi+z$ where z is the elevation, θ_s is the saturated water content. Q corresponds to
 265 the volumetric flow rate per unit volume representing a source or sink, and Γ is the exchange
 266 flux between the surface and subsurface domains.

267 The depth-integrated surface flow equation adopted in HGS involves the 2D diffusion-wave
 268 approximation:

$$269 \quad \nabla \cdot (d_o \mathbf{K}_o \nabla h_o) \pm Q_o + \Gamma_o = \frac{\partial h_o}{\partial t} \quad (2)$$

270 where d_o is the depth of flow, h_o is the water surface elevation ($= d_o + z$), and K_o is the
 271 surface conductances that is function of the friction slope of the surface and is determined by
 272 the Manning's equation in the x- and y- directions as

$$273 \quad K_{ox} = \frac{d_o^{2/3}}{n_x} \frac{1}{[\partial h_o / \partial s]^{1/2}}; \quad K_{oy} = \frac{d_o^{2/3}}{n_y} \frac{1}{[\partial h_o / \partial s]^{1/2}} \quad (3)$$

274 where n_x and n_y are the Manning's roughness coefficients and s is the direction of maximum
 275 surface-water slope. The surface conductances K_{ox} and K_{oy} are complex functions of the
 276 dependent variables d_o or h_o ($= d_o + z$), and the relationships make Equation (2) nonlinear.

277 The surface and subsurface flow equations are coupled with a third type flux equation as
 278 follows:

279 2.3.1 Flux exchange and Evapotranspiration equations

280 The individual surface and subsurface flow equations can be coupled by assuming that the
 281 two flow regimes are separated by a thin boundary layer. Thus, Γ_o represents a first-order
 282 exchange flux between the subsurface and surface domains as follows:

$$283 \quad \Gamma_o = (k_r)_{exch} K_{exch} (h - h_o) / l_{exch} \quad (4)$$

284 where $(k_r)_{exch}$ is the relative permeability for fluid exchange, K_{exch} is the surface/subsurface
 285 conductance, and l_{exch} is the thickness of the interface layer between surface and subsurface
 286 domains. In Equation (4), a positive Γ_o indicates water mass movement from the subsurface
 287 to the surface domain and vice versa for negative fluxes.

288

289 In this study, the actual evapotranspiration (AET) is computed following the approach
 290 suggested by Kristensen and Jensen(1975). Detailed information on the approach can be
 291 found in the HGS documentation (Aquanty Inc, 2017).

292 2.3.2 Groundwater recharge

293 The definition of groundwater recharge considered is the same approach followed by Erler et
 294 al.(2018); wherein groundwater recharge is derived from the HGS output of exchange flux
 295 between surface and subsurface domains as described in equations 5 and 6.

296 Equation 5 describes the groundwater recharge for a terrestrial landscape where there is no
 297 standing surface water (i.e., ponds, river, and spring).

$$298 \quad R = \Gamma_o - (Ss_e + Ss_t) \quad (5)$$

299 Where R is the groundwater recharge, Γ_o corresponds to the HGS exchange flux between
 300 surface and subsurface, and Ss_e and Ss_t are respectively the subsurface evaporation and
 301 subsurface transpiration.

302 With standing surface water such as river or ponds, groundwater recharge corresponds to the
 303 HGS exchange flux term (Equation 6).

$$304 \quad R = \Gamma_o \quad (6)$$

305 Since the exchange flux term is calculated after surface evaporation, and when standing water
 306 is present, no subsurface evapotranspiration occurs, groundwater recharge equals exchange
 307 flux where standing water (i.e., ponds) are present.

308 **2.4 Conceptual Model and Discretization**

309 The modelled study area covers both the sandstone CT3 aquifer, and the fractured
 310 Precambrian basement aquifers. An equivalent porous medium (EPM) approach is considered
 311 to represent the fractured aquifer unit in the integrated model. The first motivation in applying
 312 an EPM approach is the complexity of the fractured distribution in the study area. The data
 313 required to simulate flow in the fractured aquifer (vertical fracture distribution, spacing, and
 314 aperture) are not available, and even with these data; the spatial heterogeneity is variable and
 315 may not be well represented at the watershed scale. Since this study only focuses on water
 316 quantity, we believe that an effective representation of the fracture aquifer unit with the EPM
 317 approach is appropriate.

318 The second reason for applying an EPM approach is that, while HGS is able to simulate flow
 319 in discrete fractures, it solves the Brooks-Corey (1964) equation for both porous medium and
 320 discrete fractures in the unsaturated flow domain. The conceptual geological model
 321 (Figure2a) is composed of four hydrogeological units. The CT3 unit is represented at the top
 322 of the conceptual model and considered to be in hydraulic connection with the alluvial
 323 aquifer. As stated in section 2.2, the CT3 is conceptually represented by three different
 324 geological facies of clay, clayish sandstones, and silty sand. The fractured aquifer is
 325 characterized by three different units: The granitic formations are intrusive into the birrimian

326 schist formation (Figure 2a). However, this geological configuration is simplified in the
327 model (Figure 2b) by considering the granitic aquifer at the bottom of the model and the
328 schists aquifer at the top of the granitic layer. The third aquifer is composed of the weathered
329 formation, consisting to the undifferentiated weathering horizons of both granites and schist
330 formations.

331 *2.4.1 Boundary conditions*

332 The modeled domain corresponds to Niamey watershed as delineated by the hydrogeological
333 watershed of the city and its surrounding villages. No flow boundary conditions were
334 assigned to all outer subsurface model domain boundaries, and groundwater flow divides are
335 assumed to correspond to the hydrological watershed limits. Four additional boundary
336 conditions types were applied to the top surface of the model domain: precipitation, potential
337 evapotranspiration (PET), critical depth and surface water flux. Precipitation and PET were
338 assigned to the top of the model as hydroclimate forcing variables. A critical depth boundary
339 condition was applied at the outer edge boundary of the model to let surface water flow out of
340 the model domain. The critical-depth boundary condition is implemented to simulate
341 conditions at the lower boundaries of a hill slope. This boundary condition forces the water
342 elevation at the boundary to be equal to the water elevation for which the energy of the
343 flowing water relatively to the stream bottom is minimum (Hornberger et al., 1998; Therrien
344 et al., 2005; Aquanty, 2018). A surface water flux boundary condition was assigned at the
345 most northern point to represent the Niger River inflow coming from upstream which was not
346 generated in the modeled hydrogeological watershed. We acknowledge that the flow at the
347 surface water flux boundary condition is affected by the precipitation between the Kandadji
348 gauging station and the inlet of the model. However, we herein assume that this amount of
349 precipitation is negligible compared to the flow of the River, as Niger River flow at Niamey is
350 more influenced by the Guinean rainfall regime (1400mm/year) than Sahelian rainfall (400
351 mm/year) as previously shown by Amogu et al, (2010) . We therefore assumed that the flow
352 at the Kandadji station could reasonably represent the flow at the inlet of the model as the
353 area between Kandadji and the inlet of the watershed still under Sahelian rainfall regime.

354 *2.4.2. Model Discretization*

355 The surface domain of the model was discretized into triangular mesh elements with a
356 resolution ranging from 300 m on average to 70 m near surface flow features. The subsurface
357 model consists of triangular prism-shaped elements which are each defined by 6 nodes. The

358 model has eleven layers with a total of 516,901 nodes, and 927,030 elements. In order to
359 represent the surface water-groundwater exchange and evapotranspiration processes more
360 accurately near the top surface, the first three meters were discretized vertically into five
361 layers at 0.1, 0.15, 0.25, 0.5 and 1.5 meters resolution. The interpolated geological materials
362 from the boreholes were used for the remaining six lowest bedrock layers. The digital
363 elevation model (DEM) of 30 m x 30 m was used to assign elevations to the top most 2D
364 layer. The DEM was hydrologically corrected to avoid artificial lakes along stream channels
365 by modifying nodal elevations to decrease from upstream to downstream.

366 **2.5. Calibration Approach**

367 The calibration procedure adopted in this study is done in three steps (Figure 3).

368 **Step 1: Steady State Calibration**

369 The steady state calibration involved forcing the model with a 30 year (1980-2005) long-term
370 average net precipitation and potential evapotranspiration. The net precipitation was
371 calculated based on the increase in average stream flow across the study area (Equation 7):

372

$$373 \quad P_{net} = (Q_{in} - Q_{out}) / A \quad (7)$$

374 where P_{net} is the net precipitation, Q_{in} corresponds to the river inflow, and Q_{out} is the
375 surface water outflow, at the outer edge of the basin and A represents the surface area the
376 watershed between the Kandadji and Niamey stations. The detailed equations of net
377 precipitation calculation in integrated hydrological models are provided in Hwang et al.,
378 (2014). This approach enables also to take into consideration the inflow part of the river
379 hydrograph that is not generated due to local precipitation, and also to better represent the
380 river aquifer interaction at the early stage of the model calibration.

381

382 **Step 2: Dynamic Equilibrium**

383 The second model calibration step is intermediate between steady state and daily transient
384 simulations referred here as dynamic equilibrium. It consists of forcing the model with
385 monthly normal precipitation and PET and while using steady state results as initial

386 conditions. Essentially, the long-term hydro climate forcing data (1980-2005) used to force
387 the model are aggregated into one synthetic year of twelve months, representing the average
388 seasonal cycle. The monthly normal forcing data are considered to represent the long-term
389 average seasonal cycle. This forcing data is repeatedly applied to the model until dynamic
390 equilibrium is achieved. Dynamic equilibrium is determined to have been reached when no
391 significant variations of the river and groundwater hydrographs are observed from year to
392 year. This approach has the advantage of training the model from theoretical steady state to a
393 more naturally occurring transient conditions represented by the monthly normal forcing. It is
394 particularly important for the dry climate conditions, where monsoonal intermittent
395 precipitations are driving the hydrological cycle and will allow for providing reasonable
396 initial conditions to the daily transient simulations. The dynamic equilibrium is considered
397 here to be a transitional state much closer to natural equilibrium than a traditional steady state
398 conditions (Erler et al., 2018).

399

400 The model state at the end of the dynamic equilibrium is then used as an initial condition for
401 the daily transient simulations. The daily transient is run for the period of 2011-2017 where
402 continuous groundwater observation data are available. Manual calibration was performed by
403 trial and error until a satisfactory match was achieved between simulated and observed
404 groundwater heads and surface water flow rates.

405

406 **Step 3: Daily Transient Calibration**

407 The initial conditions at the end of the dynamic equilibrium are then used to force the model
408 for the daily transient simulations. The daily transient is run for the period of 2011-2017
409 where continuous groundwater observation data are available. Manual calibration was
410 performed until a satisfactory match was found between simulated and observed groundwater
411 head, and surface water flow rate.

412 The Hydrologic parameters used for the simulation at the steady state (step1) are provided in
413 Table 1. Calibration at the dynamic equilibrium and transient simulations steps further show
414 that model is only sensitive to the parameters provided in the Tables 2 and 3. Therefore, the
415 calibration at dynamic equilibrium and transients conditions was performed by manually

416 adjusting the sensitive parameters (Tables 2 and 3) to both groundwater and surface water
417 flow rates, representing the objective function.

418 Also, during the model calibration, we have first used the average long term precipitation and
419 observed PET at Niamey climate station (shown in Figure 1), but the resulting hydrologic
420 regime was too dry. This is because, the intermittency of precipitation is lost, and average
421 PET will always be greater than precipitation and the system will dry completely. The equation
422 7 represents a methodological approach of spinning up model at the early stages of calibration
423 in such a dry (Sahelian) rainfall regime.

424 **3. Results and Discussion**

425 **3.1 Parameter estimation**

426 *3.1.1 Hydraulic conductivity and Van Genuchten parameters*

427 Calibrated hydraulic conductivity (K) values, residual water saturation and van Genuchten
428 parameters for the different hydrogeological units are shown in Table 2. The CT3 aquifer,
429 which is pinching out over the basement aquifer, has a calibrated hydraulic conductivity of
430 1.12×10^{-5} m/s. This value agrees well with the calibrated value from Favreau (1996) for the
431 CT3 aquifer at the Wankama site. No previous studies have estimated the K of the
432 Precambrian basement aquifers. Calibrated K values (Table 2) for the Precambrian basement
433 aquifers are generally within the literature reported range (Domenico and Schwartz, 1990).
434 The calibrated K of the granitic aquifer is one order magnitude greater than the calibrated
435 value for the schist aquifer (Table 2). The calibration process also revealed a structural control
436 on the K values for different hydrogeological units. The calibration process further showed a
437 kind of geologic and or structural control on the hydraulic conductivities values for different
438 hydrogeological units. Although this control depends on very localized geologically
439 phenomenon (fracture density, weathering process), the granitic aquifer, when altered
440 mechanically and or fractured, has a higher K than the schist aquifer, of which the alteration
441 products are generally composed of clayey materials, and are less likely to fracture.

442

443

444 *3.1.2 Evapotranspiration and overland flow parameters*

445 Calibrated actual evapotranspiration and overland flow parameters are presented in Table 3,
446 for each land use type. Maximum Leaf Area Index values range from 0.01 for urban area, to
447 1.25 for Savanna, with Agriculture and Steppe having the same maximum LAI values of 1.2.
448 Root depth values for Savanna (4.5 m) are three times more than for agriculture (1.5m), with
449 steppe having a root depth value of 1 m. Root depth of urban and bare soil land use are
450 respectively of 0.1, and 0.01 meters. The calibrated root depth values of savanna and
451 agricultural land are in good agreement with values presented in Ibrahim et al. (2014).
452 Calibrated Manning friction coefficients for overland flow range between 0.016 to 0.43 ($s \cdot m^{-1/3}$)
453 for different land use types, and coupling length values range from 0.01 to 0.1 m (Table
454 3).

455 **3.2. Comparison of simulated and observed hydraulics heads and surface water flow** 456 **rates**

457 Long term steady state calibrated groundwater heads for 25 observations wells are plotted
458 against available long term measured groundwater heads for both the CT and Fractured
459 aquifer (Figure 4 a). The long term average period considered is 1980-2005, and simulated
460 groundwater heads reasonably approach the observed head with an R^2 value of 0.82. The level
461 of agreement between groundwater heads for the fractured aquifer is higher than for the CT,
462 because a higher weighting was placed on the fractured aquifer calibration performance as it
463 has more reliable long term groundwater heads measurements. The steady state calibration is
464 the first step of the calibration approach followed by the dynamic equilibrium calibration, for
465 groundwater heads (Figure4b) and surface water flow rates (Figure 4c). The simulated
466 seasonal cycle of groundwater heads (Figure4b) at Kossey Djerma observation well after 15
467 years of monthly normal simulations follows the measured groundwater heads reasonably
468 well, but with a time lag bias in the simulated hydraulic heads. Calibration further showed
469 that groundwater wells located near the river reached the dynamic equilibrium more rapidly,
470 within 10 years simulation, more than 10 years was required for wells that are further from
471 the river. Also, surface water flow was found to stabilize in less than 2 years of simulation,
472 similar to the findings of Goderniaux et al. (2009). The calibration of monthly normal
473 groundwater levels show good agreement with observed groundwater levels for both mean
474 values and seasonal amplitude, however, a time lag bias is present in the simulated heads
475 which is suspected to be a result of the EPM conceptualization of the fractured rock aquifer.
476 The time lag bias between the simulated and observed groundwater levels for the Dynamic
477 Equilibrium calibration step were not rigorously addressed to avoid overfitting, and to

478 maintain calibrated values within physically reasonable ranges. The simulated seasonal cycle
479 of surface water flow rates at Niamey station are in good agreement with observations
480 (Figure 4c), with both river peaks during the local rainy season and of the inflow from
481 upstream well captured by the model with a slightly positive bias during the peak of
482 September. In fact calibrating integrated hydrological models with both surface water flow
483 rate and groundwater wells is not a very common practice (Goderniaux et al., 2009; Jones,
484 2005; Li et al., 2008; Sudicky et al., 2008) in integrated hydrological model calibration, and
485 as the calibration level will allow to reasonably reach the objective of the model development
486 (water balance, GW-SW) considering the EPM approach, the monthly normal calibration
487 results are considered satisfactory and are used as initial conditions for daily transient
488 simulations (Figure 5).

489 Daily transient simulations results for three observations wells that have available
490 groundwater head measurements (Figure 5) show acceptable agreement between observed
491 and simulated groundwater heads for 5 years (2013-2017). The first two years (2011-2013)
492 are considered as model spin up period. The three observation wells (Figure 5) are located in
493 the fractured aquifer, because no continuous groundwater measurements heads are available
494 for the CT aquifer. Compared to the monthly normal simulations, simulated daily transient
495 groundwater heads have less time lag, and in all the three wells, simulated mean heads
496 approach the measured heads very closely. The time lag bias observed from daily transient
497 wells is different for the three observations wells, implying highly variable hydraulic
498 conductivities in the fractured aquifer, controlled by localized geological features (fractures
499 density, aperture, weathered zone thickness) that the current EPM conceptualization of the
500 model may not be able to capture. The EPM representation appears to be useful in regional
501 groundwater flow system characterization, but may be too simple to capture the complexity of
502 local geological conditions (Anderson and Woessner, 1992).

503 In order to improve the calibration results of groundwater heads, especially the observed lag
504 between simulated and observed groundwater levels in the transient simulations, advanced
505 model calibration methods using pilot points may be used. This method would allow the use
506 of spatial heterogeneities in the sensitive hydrologic parameters for improving the objective
507 function. Detailed information and a tutorial on this advanced calibration method can be
508 found in Moeck and Brunner (2014).

509 Daily transient simulated surface water flow rates at the Niamey gauge (Figure 6) are
510 relatively well reproduced by the model, with the local flow peak (rainy season) and Guinean
511 flow peak captured in August and December respectively.

512

513 **3.3 Exchange flux**

514 The simulated exchange flux from five years of daily transient simulation (2013-2017) has
515 been aggregated into monthly normal exchange flux (Figure 7) in units of mm/day. Positive
516 values (red) represent the exfiltration from the porous medium to the surface, while negative
517 values (blue) correspond to the water infiltrating from the surface to the subsurface. The 2D
518 spatial representation of the exchange flux is used to qualitatively characterize the process of
519 exchange between the surface water bodies and the aquifer system. The distribution of the
520 exchange flux values (Figure7) shows that the model is able to reproduce the importance of
521 the monsoonal rainfall in groundwater infiltration occurring only in the rainy season. July and
522 August are the most important periods of infiltration with an average value of up to 8
523 mm/day. In June and September, infiltration is localized at the right bank of the Niger River
524 (upstream) where irrigation occurs. The rest of the season is dry, and there is no infiltration.
525 Groundwater exfiltration shows different patterns depending on the surface water bodies
526 considered. The Niger River acts as a gaining stream where groundwater exfiltrates to the
527 river during the rainy and dry seasons. Although, it is clear that the River is gaining, the
528 exfiltration rates are very small, relative to the total flows in the river, and the process is only
529 important for few months of the year (August, February and March). Using a piezometric map
530 of Niamey, Hassane et al. (2016), have already shown the CT aquifer discharges to the Niger
531 River which agrees with this study.

532

533 Considering the ponds and ephemeral streams, the exchange flux processes are a bit more
534 complex, and result from more local hydrogeological conditions (topography, hydrologic
535 conductivities), with some ponds acting as depressions focused recharge areas and others as
536 groundwater discharge area. The channels of the ephemeral streams are predominantly
537 groundwater discharge areas while the main stream course is mainly a recharge area. This
538 phenomenon of ponds and parts of ephemeral streams acting as groundwater discharge zones

539 may be related to the recent changes of land use resulting in the creation of temporary ponds
540 (Favreau et al., 2009; Mamoudou et al., 2015).

541 While monthly normal exchange fluxes provide a qualitative understating of the seasonal
542 cycle of river-aquifer exchange (Erler et al., 2018), they do not carry sufficient temporal
543 resolution to quantify and understand the highly transient relationship between surface and
544 subsurface exchanges fluxes for this dry environment with intermittent precipitation. For this
545 watershed daily exchange fluxes are required (Figure 8)

546 Daily time series of exchanges flux have been derived at multiple locations (Figures 8 and 9)
547 in order to characterize the surface water groundwater interactions depending on the type of
548 the surface water features considered (i.e., Niger River, ponds, ephemeral stream)

549 Figures 8a and 8b show the daily time series profile of ponds-aquifer exchange flux for the
550 Zarmagande pond and Koungou pond respectively. Exchange flux at Zarmagande pond
551 (Figure 8a) is dominated by groundwater discharge during the rainy season (July to
552 September), and by groundwater recharge in the dry season (October to June). In the rainy
553 season, when groundwater is discharging into the ponds, the volume discharging into the
554 pond is more important during intense rainfall events (Figure 8a) with an exfiltration rate of
555 up to 40 mm/day, which is considerably greater than actual evapotranspiration rate of 2 -3
556 mm/day. In contrast, infiltration of up to 20 mm/day may occurs from pond to aquifer during
557 the dry season, which lead to about 17to 15 mm/ day of recharge after removing actual
558 evapotranspiration rate (3to 5 mm/day). At Koungou pond (Figure8b), located 500 m away
559 from Zarmagande pond , at a lower altitude , the exchange flux is exclusively characterized by
560 infiltration of pond water into groundwater. The infiltration rate, which is dependent on
561 rainfall intensity, can reach up to 50 mm/day during intense precipitation events (i.e., 120
562 mm/day). The difference in the exchange flux of the two ponds may be related to local
563 topography, with Zarmagande pond located in a topographically low area (196 m.a.s.l), and
564 Kongou pond, at greater elevations (201 m.a.s.l). Furthermore, the phenomenon of
565 groundwater discharge into ponds, may be a result of recent land use change and climate
566 induced groundwater table rise well documented in the study area from rural zones (Favreau,
567 2000; Favreau et al.,2009) to urban area(Hassane et al., 2016).

568 While there is significant groundwater recharge in the vicinity of the two ponds, there is a
569 qualitative difference to the spring at Gounti Yena (Figure 8c) where the exchange flux is
570 characterized by a continuous groundwater discharge throughout the year. The main peak of

571 the exfiltration occurs during the late rainy season and decreases during the dry season. The
572 more intense the rainfall event is, the greater the exfiltration rate. During the late dry season
573 (May, June) and early rainy season (July), little infiltration occurs, as evapotranspiration is the
574 dominant process and considerably reduces the amount of water available to infiltrate. The
575 ephemeral stream, Gounti Yena, is a groundwater discharge area, and its discharge rates can
576 serve as a precursor to groundwater flooding especially during extreme precipitation event.
577 Another ephemeral stream at Gorou Kirey shows a different exchange flux behavior (Figure
578 8d) with surface water infiltrating into groundwater and producing a significant groundwater
579 recharge.

580 Figure 9 shows exchange flux time series between the Niger River and the underlying aquifer
581 at two locations, to characterize groundwater-surface water interactions. The time series
582 (Figure 9) are considered to represent the main types of interactions in the vicinity of the
583 permanent river in the study area. The simulation results further show that when there is a
584 significant interaction between the river and underlying aquifer, the river is acting as either
585 gaining, or losing stream depending on the zone considered. While the monthly normal
586 exchange flux discussed earlier showed the Niger River to mainly have a gaining stream
587 profile, the daily exchange flux time series allows for a more detailed profile.

588

589 Therefore, Niger River acts as losing stream in some zones (Figure 9a), and gaining stream
590 (Figure 9b) in others zones. In general, the losing zones are located near faults zones, where
591 fractures are dense, and allow significant surface water infiltration into groundwater. One
592 important aspect to notice is that no infiltration occurs during the Guinea river peak flow from
593 November to February. Infiltration occurs only during the rainy season, during the local peak
594 of the river, resulting in groundwater recharge of up to 50 mm/day during intense rainfall, as
595 actual evapotranspiration (Figure 9a) is low during these events, allowing significant
596 groundwater recharge to occur. However, the losing zones of the river are only localized near
597 important fractures zones, and in most area, models results do not show significant infiltration
598 processes in other zones of the river. It is also worth noting that the infiltration rate of river
599 water is more dependent on the intensity of individual rainfall events, than the mean monthly
600 or annual rainfall. The importance of fractures zones in groundwater recharge has been shown
601 by Girard (1993) for this study area using hydrochemicals and isotopes methods.

602 Apart from above mentioned localized fractures zones where the river water recharges
603 groundwater, the remaining part of the Niger River is gaining from underlying aquifer
604 (Figure9b). The exchange flux profile at gaining parts of the river (Figure9b) is dominated by
605 groundwater exfiltration in the rainy season, with an exfiltration rate of up to 20 mm/day.
606 This exfiltration rate results in baseflow of up to 15 mm/day when actual ET (less than
607 5mm/day) is considered (Figure 9b), and shows two peaks, one at the end of the dry period
608 (April –May), and another in the earlier rainy season (June-July). This shows that
609 groundwater is sustaining the baseflow of the river during the dry season, and at the beginning
610 of the rainy season. The exfiltration rate then decreases from the middle of the rainy season
611 (August) to reach zero by the end of the Guinea high peak flow period (November-February).
612 This is because groundwater heads are almost always above the Niger River levels (Hassane
613 et al., 2016), and particularly, during the dry period. Figure 9b also shows that there is slight
614 infiltration occurring during the high Guinea flow of the river resulting in low groundwater
615 recharge rate (less than 5 mm/day). The Niger River peak that is generated by the Guinea flow
616 peak upstream, in the upper Niger basin does not contribute to groundwater recharge in the
617 study area. This may be explained by the relatively slow flow of the Guinea flow compared to
618 the local flow peak, which is characterized by intermittent precipitation flashy stream flow
619 behavior.

620 In order to confirm the relative position of the Niger River to groundwater, 3D map of the
621 depth to groundwater table (Figures 10a and 10b) and groundwater heads (Figures 10c and
622 10d) are shown for different seasons of the year. During the dry season, the depth to the
623 groundwater table ranges from less than 5 meters near the Niger River and ephemeral streams
624 (Figure10a), to 65 meters in topographically high areas. In most areas the groundwater table is
625 at a shallow depth during the rainy season (Figure10b).

626 Both depth to groundwater table and groundwater heads show the topographical control on
627 the groundwater flow system. The Niger River as well as many ephemeral streams act as
628 natural groundwater discharge areas. A good illustration of the seasonal variability of
629 groundwater flow is shown in the Figure 10c and 10d. Groundwater heads during the dry
630 season (Figure 10c) are almost always less than model calculated heads during the rainy
631 season where many piezometric domes appeared as a combined effect of topographical
632 control and groundwater table rise (Figure 10d) . The observed heads difference is a result of
633 groundwater recharge occurring in the rainy season.

634

635 **3.4 Water balance**

636 This modelling work has highlighted that different surface water features (i.e., ponds,
637 ephemeral stream, the Niger River, and springs) exhibit different type of exchange flux
638 profiles. In this section, the water balance for different land use types will be presented as
639 well as the basin average water balance. We also qualitatively present model calculated
640 recharge for different land use types which is one of the most problematic parameters to
641 estimate in semi-arid climate (Simmers, 1997).

642

643 *3.4.1 Water balance by land use type*

644 The different land use types considered as along with relevant water balance components are
645 presented in Table 4. Ponds that are similar to Zarmagandé pond (ponds type 1), discussed in
646 section 3, have a recharge rate of up to 203 mm/year, and a discharge from groundwater
647 reaching 213 mm/year. The infiltration rate calculated from the exchange flux is 203 mm/year
648 and is assumed to represent groundwater recharge because the surface evaporation
649 representing the main ET process is removed in the exchange flux. The total actual ET
650 represented mainly by surface evaporation is of 101 mm/year. Groundwater recharge at the
651 vicinity of the pond type 2 (Koungou pond) is 174 mm/year, with total actual ET (mainly
652 surface evaporation) of 97 mm /year (Table 4). However, the recharge values calculated here
653 are point values (less than a m²); in order to qualitatively understand the exchange flux profile
654 at the vicinity of the ponds. Previous studies (Favreau, 1998; Disconnets et al., 1997) have
655 highlighted the strong spatial and temporal variability of focused recharge near ponds,
656 depending on the size of the ponds drainage area, which is critical to exactly compute in an
657 endoreic basin (Favreau, 2000).

658 Groundwater infiltration at agricultural sites is 119 mm/year, with total actual ET of 51
659 mm/year and groundwater recharge of 68 mm/year. In contrast, no groundwater recharge was
660 recorded at Savanna site, where total ET is greater than the infiltrated water (93 mm/year).
661 While, the infiltration values of agriculture and Savanna land use are in the same order of
662 magnitude (119 and 93mm/year respectively), and consistent with measured values (160 –290
663 mm/year) by Rockstrom et al. (1998) under millet fields at 1.8 m depths, Total actual ET of
664 Savanna (101 mm/year) is twice the actual ET of agriculture. The main reason for this

665 difference is probably the temporal activity of the root as well as the root depths. Agricultural
666 land use is characterized by millet and/or maize crops, with average root ET activity lasting 3
667 months (only during the rainy season) and a root depth of 1.5 m, while the Savanna consist of
668 shrubs that transpire continuously throughout the year and have a root depth of more than 5
669 m.

670 Ephemeral streams can have a groundwater infiltration rate of up to 70 mm/day, resulting in
671 groundwater recharge of the same rate and total ET of 49 mm/year. In contrast to ephemeral
672 streams that always act as depressions focused recharge areas (Table 4), ponds act either as
673 groundwater recharge areas or groundwater discharge zones.

674 *3.4.2 Basin average water balance*

675 The basin average water balance (Table 5) is computed from HGS water balance output file,
676 and averaged over the study area. The calculated five years (2013-2017) basin average
677 groundwater recharge is 28 mm/year representing 4.92 % of the total mean annual rainfall
678 (580 mm). Total actual evapotranspiration over the basin is 386 mm/year, accounting for 66%
679 of the total rainfall. The total ET is highly dominated by transpiration, which is 58% of the
680 total ET, while surface evaporation is only 8.65 %. Infiltration over the basin represents 15.9
681 % of the water balance and overland flow constitutes 10.91%.

682 Simulated groundwater recharge (28 mm/year) is consistent with previous recharge rate of 36
683 mm/year found by Hassane et al. (2016) using a water table fluctuation method, considering a
684 value of 1.2 m of water table rise. Favreau, et al., (2009) estimated a net groundwater recharge
685 rate of 25 ± 7 mm/year using combined water table fluctuations and geophysical methods, 50
686 km east of the study area.

687 Actual evapotranspiration as simulated by HGS is in agreement with previous measurements
688 and modeling results, focused on millet and fallow sites with total actual ET in the range of 50
689 to 44% of total rainfall (Ibrahim et al., 2014), and up to 65% to 45% (Boulain et al.
690 2009; Ramier et al., 2009) for fallow and millet respectively.

691

692

693

694

695

696

697

698 **4. Conclusion and Perspectives**

699 An equivalent porous medium approach was used to characterize groundwater surface water
700 interaction in geologically complex fractured and sedimentary aquifers, with a high resolution
701 fully integrated surface-subsurface hydrological model. The finite element HydroGeoSphere
702 model has a horizontal resolution ranging from 300 m to 70 m and eleven vertical layers
703 resulting in a total of 516901 nodes and 927030 elements. The model was calibrated using a
704 3-step methodology: 1) steady state, 2) dynamic equilibrium and 3) daily transient. The model
705 results allowed for both a qualitative and quantitative evaluation of groundwater-surface water
706 interactions for different land uses categories. In general, the groundwater flow system is
707 controlled by local topography, and the Niger River showed mainly a gaining stream profile
708 with groundwater discharge rate of up to 20 mm/day in the rainy season. However, the river
709 may act as losing stream near main faults, with an infiltration of up to 50 mm/day during
710 intense rainfall events. Ephemeral streams occur in areas of focused groundwater discharge,
711 while ponds exchange flow profile is controlled by local topography, and they act as
712 groundwater recharge or discharge areas. Significant groundwater recharge occurs in
713 agriculture /fallow land use, in contrast of Savanna where all the infiltrated groundwater are
714 lost by intense evapotranspiration processes. The calculated 5 years average groundwater
715 recharge over the basin is 28.6 mm/year with actual evapotranspiration accounting for 66.31%
716 of the total mean annual rainfall (580 mm), and slight groundwater contribution to baseflow
717 (1.66%).

718 Large scale integrated hydrological models have attracted considerable interest over the past
719 10-15 years, largely due to better availability of input data and high-performance computing
720 capacity (Bergand Sudicky,2018). The study described here confirms that the application of
721 fully integrated hydrological models to address real world problems is feasible, even with
722 modest computing resources and in regions where less data is available. While most
723 developing countries are facing challenges in water resources management, due to high
724 population growth combined with climate change, we have demonstrated that integrated

725 hydrological models help to address some of these water management challenges. Integrated
726 hydrological models constitute a useful tool for helping developing countries achieve
727 successful integrated water resources management.

728

729

Journal Pre-proof

730 **Figures and Tables**

731

732

733

734

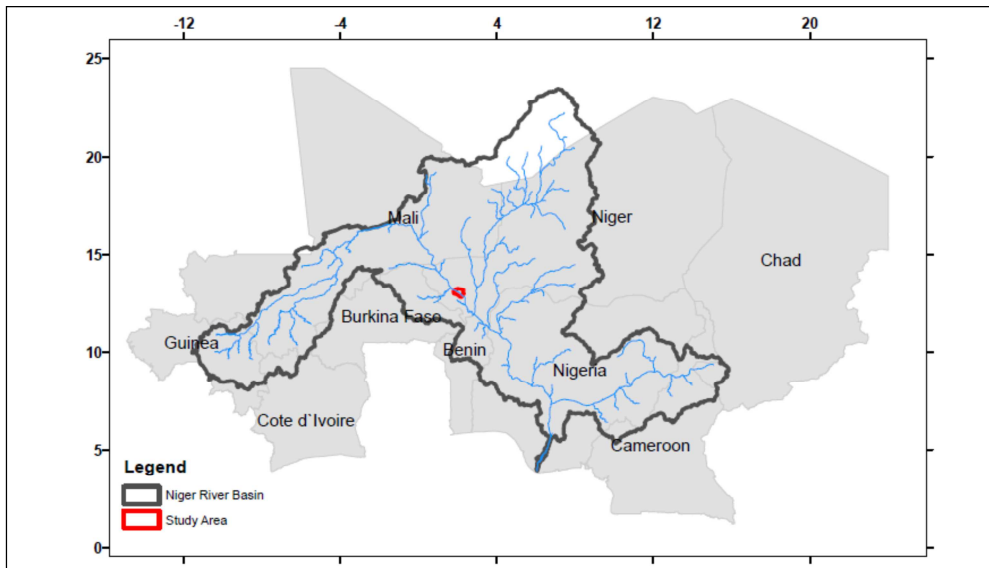
735

736

737

738

739



740 Figure 1a: Study area location within the Niger River basin

741

742

743

744

745

746

747

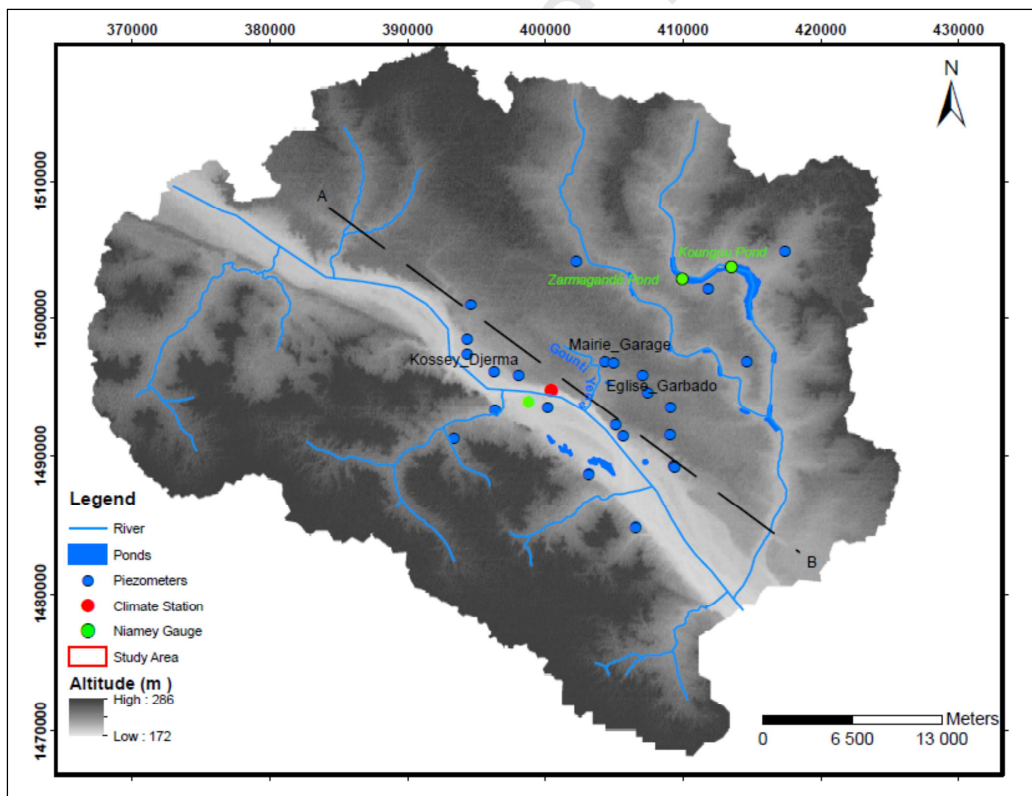
748

749

750

751

752



753 Figure 1b: Local context of the watershed, black dashed line is the x-section location shown
754 in Figure 2

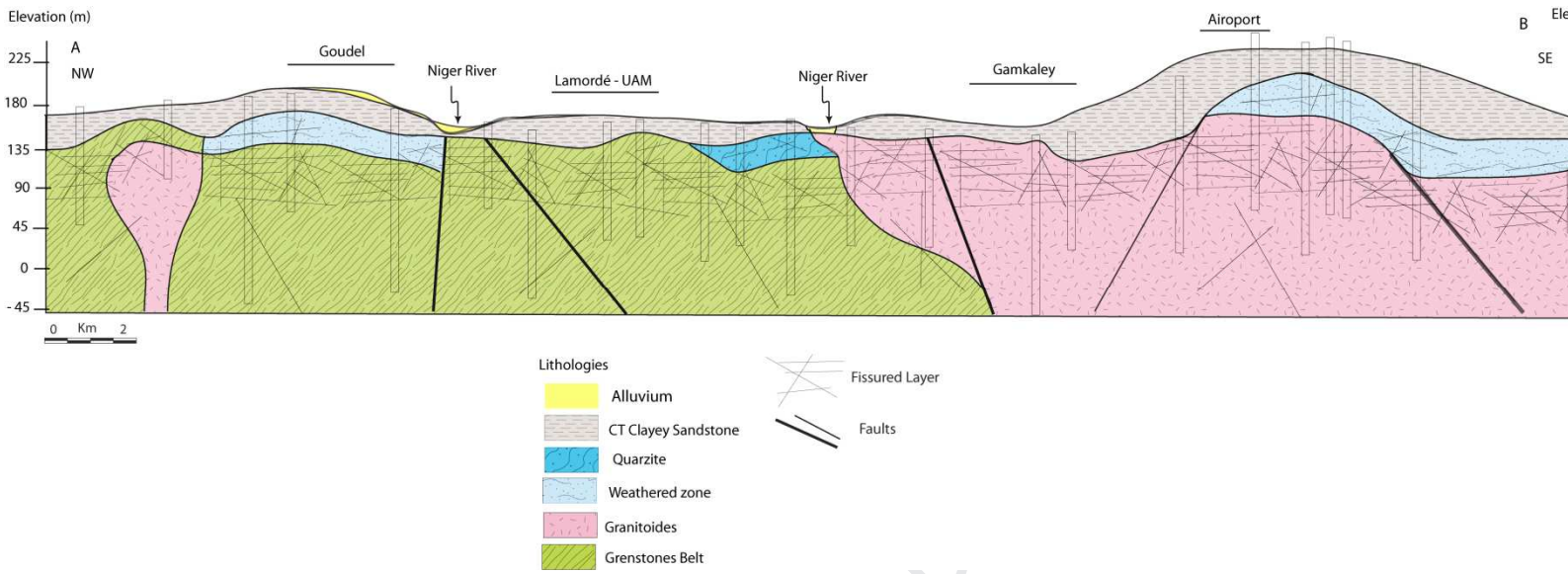
755

756

757

758

759



760

761 Figure 2a: Conceptual model representing the Hydrogeological conditions in the study area

762

763

764

765

766

767

768

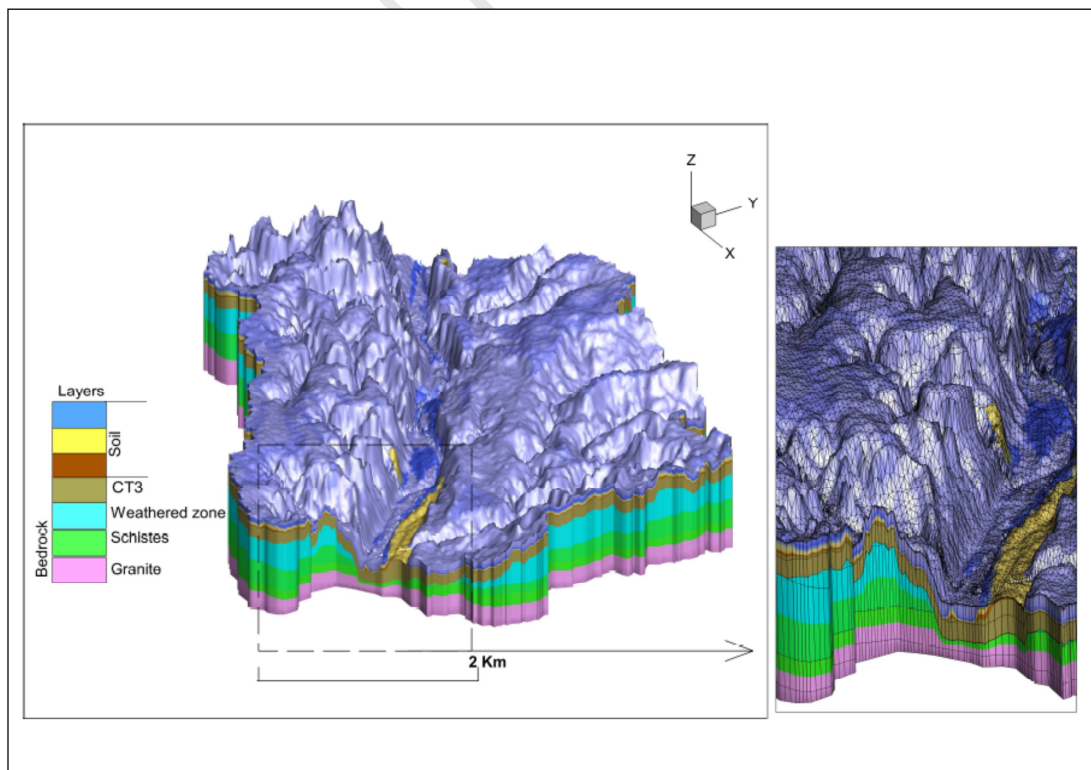
769

770

771

772

773



774

775

775 Figure 2b: 3D surface-subsurface model of the study area

776

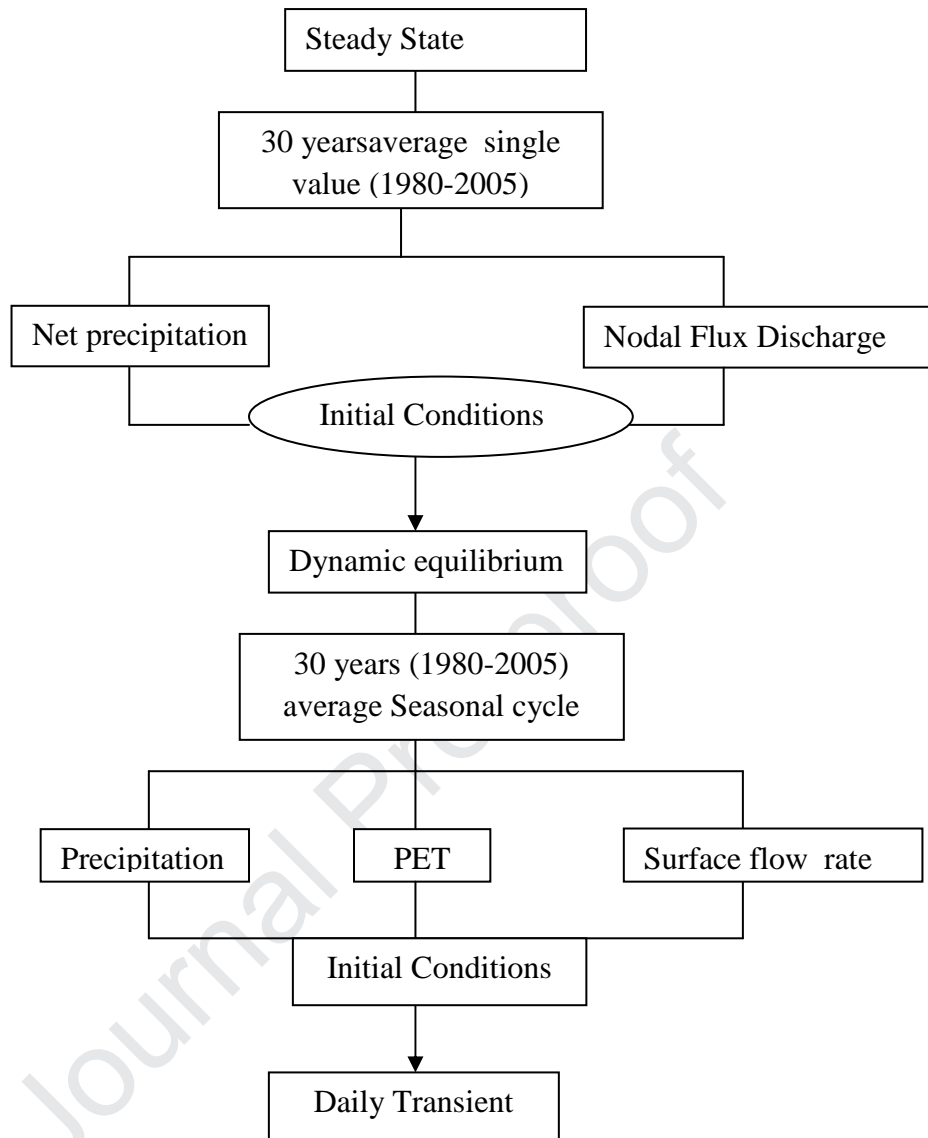
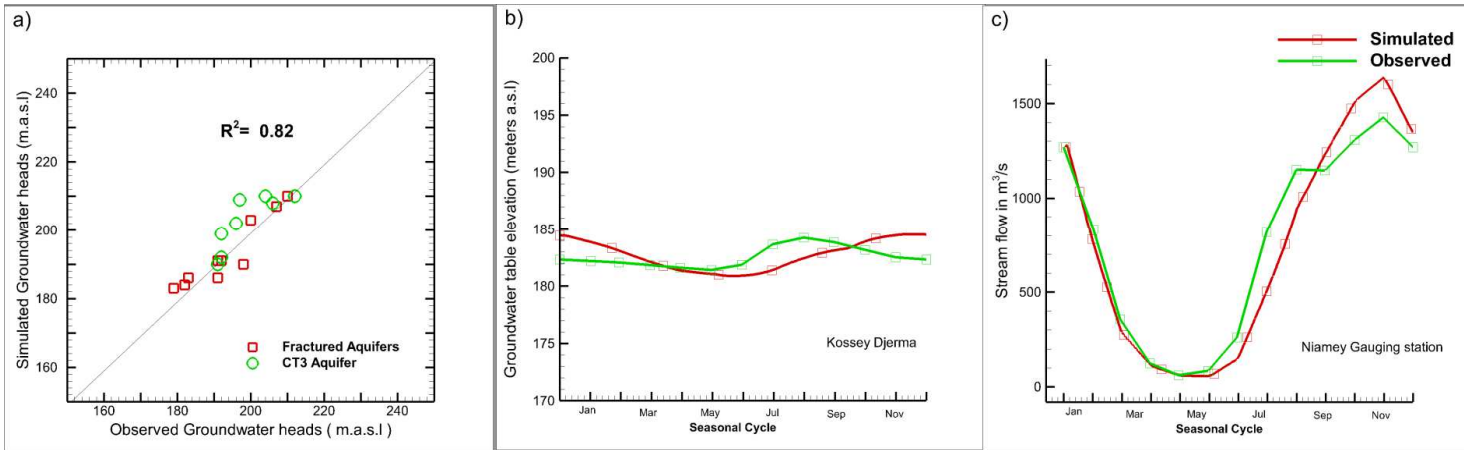


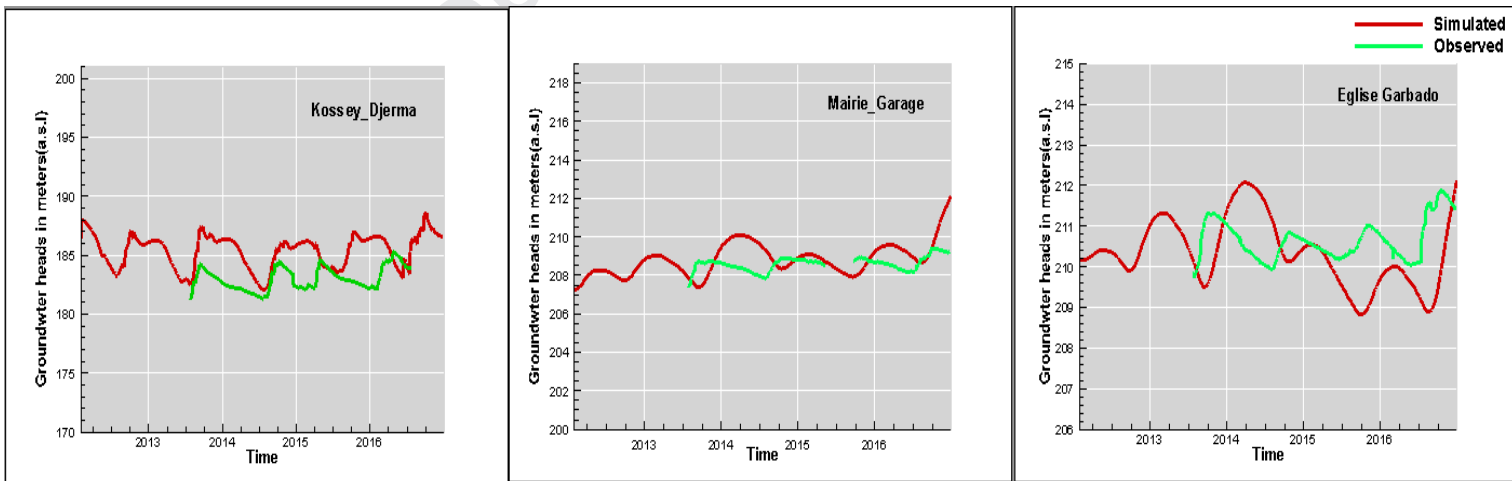
Figure 3: Calibration method flow chart

804
805
806
807



808
809
810
811
812
813

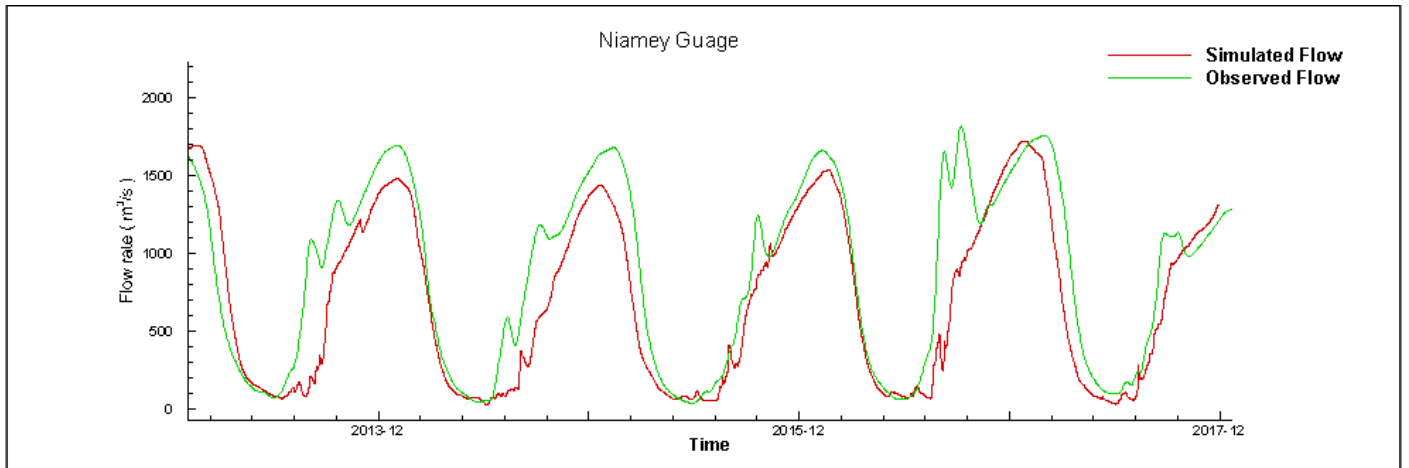
Figure 4: Steady state (a) and groundwater head calibration under dynamic equilibrium (b) and surface water flow rate calibration under dynamic equilibrium (c)



814 Figure 5: Comparison of simulated and observed daily transient groundwater heads

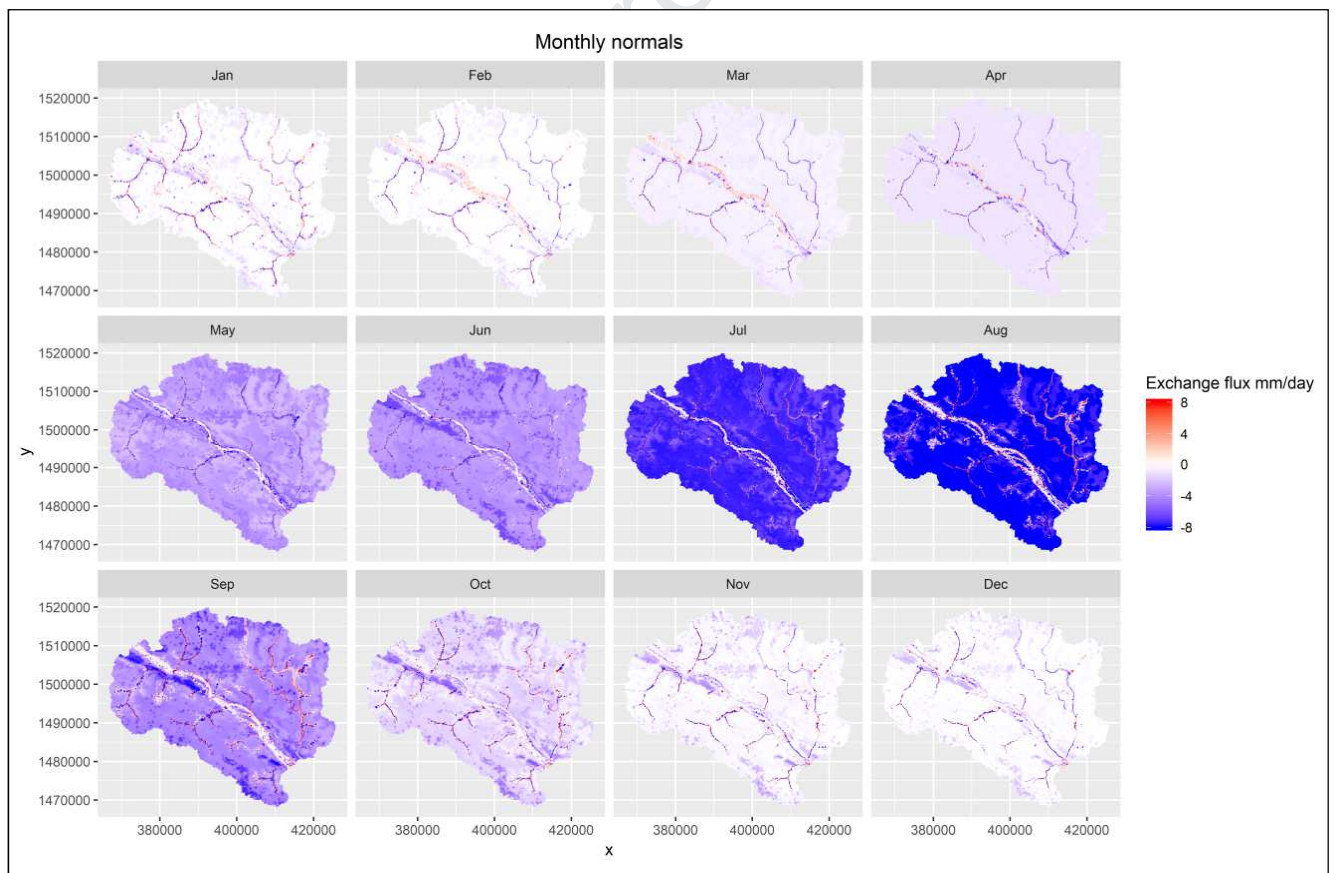
815

816



817 Figure 6: Comparison of simulated and observed daily surface water flow rate at Niamey
818 gauge

819



820

Figure 7: 2D spatial monthly normals Exchange flux

821

822

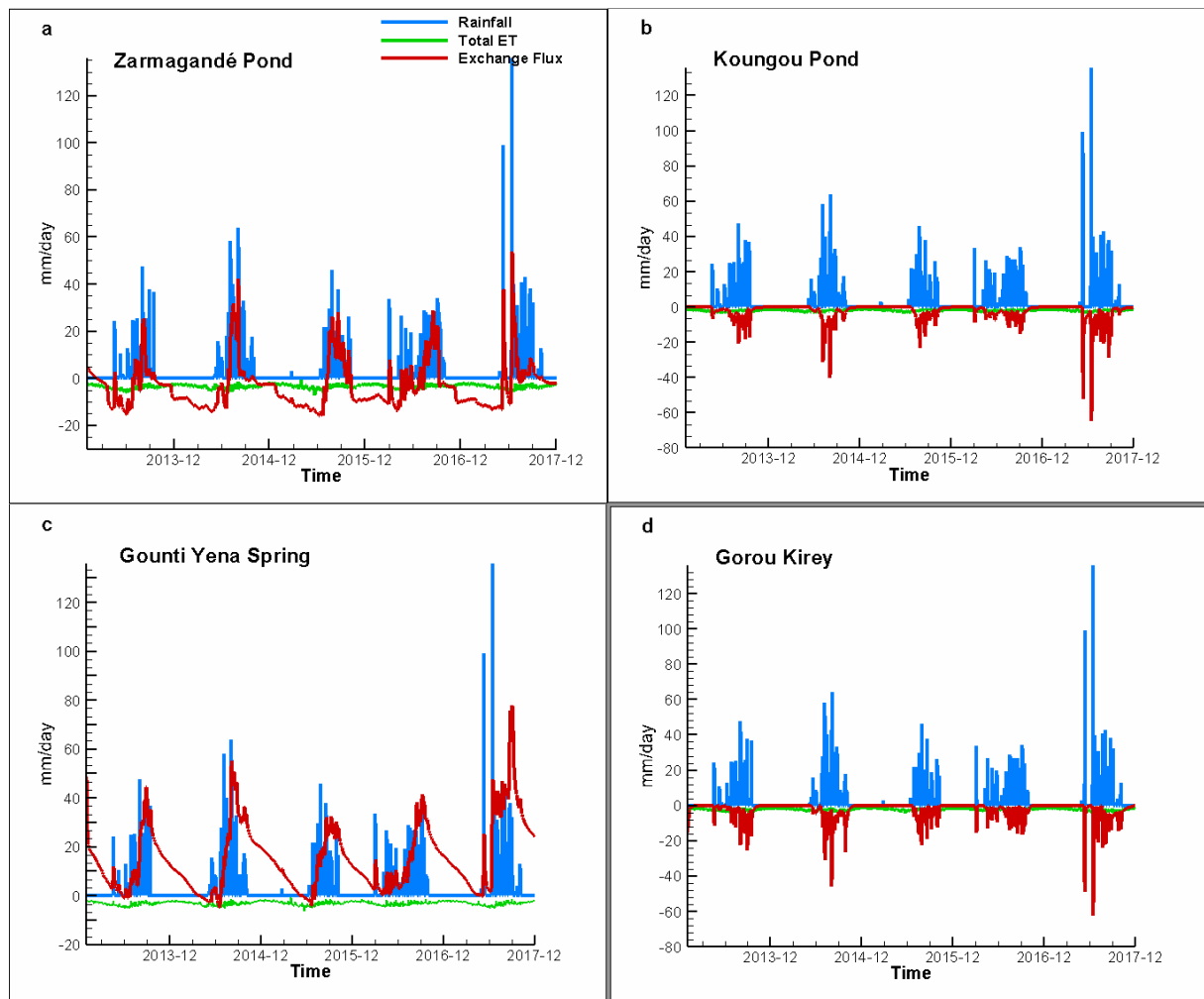
823

824

825

826

827

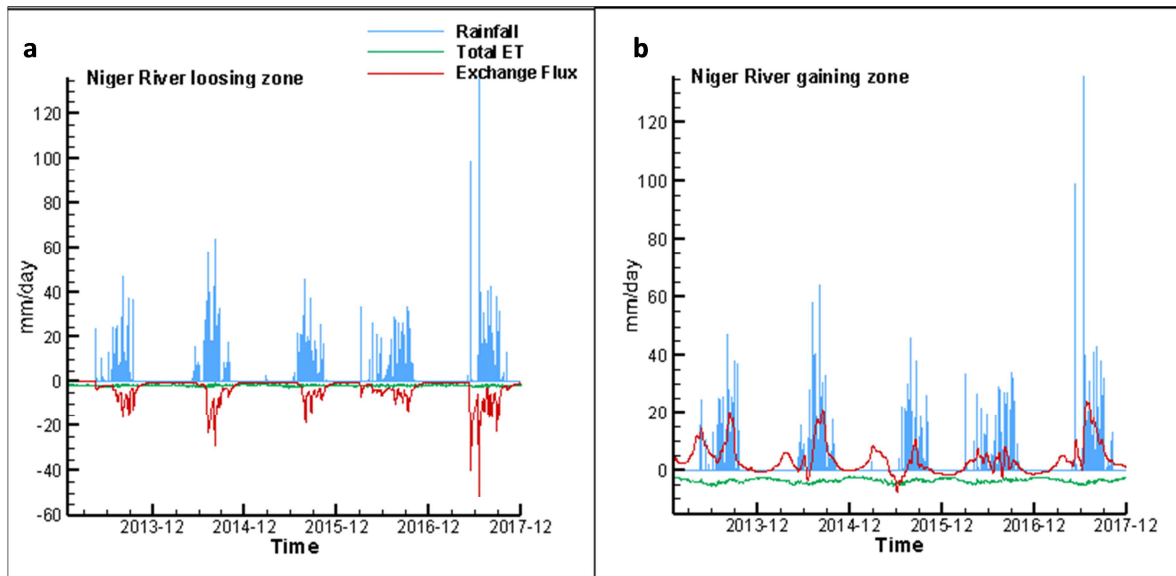


828

829

Figure 8: Exchange Flux profile for ponds (a, b) and Ephemeral Stream (c,d)

830



831 Figure 9: Exchange Flux at Niger River showing losing (a) and gaining zone (b) profiles

832

833

834

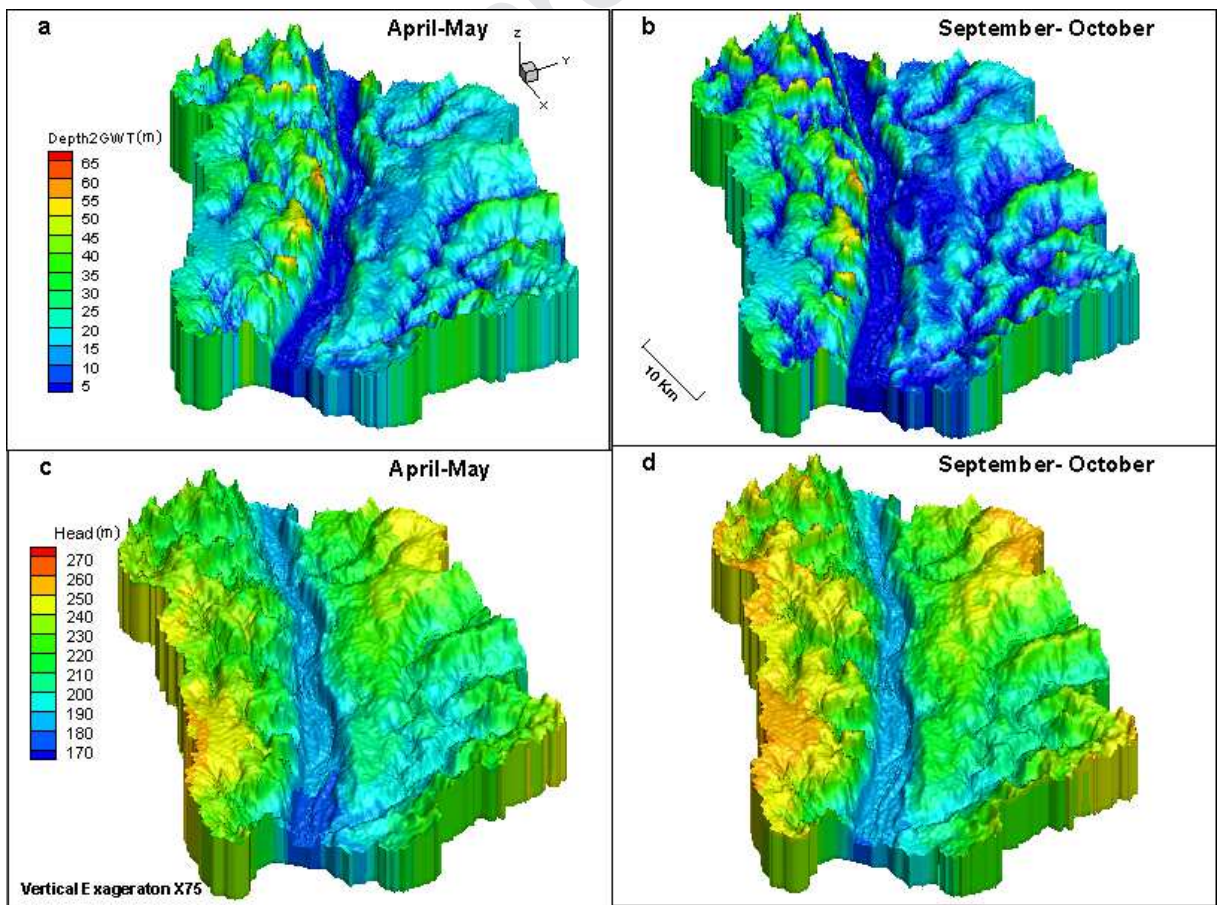
835

836

837

838

839



840

841

842

843

844

845

846

847 Figure 10: Simulated 3D Spatial Depth to groundwater table (a, b) and groundwater heads (c,
848 d) at different periods

849

850

851 **Table 1:** Hydrologic parameters used at the steady state step

Parameters	Symbol	Units
Saturated hydraulic conductivity	K	[m/s]
Total porosity	n	[-]
Specific storage	S_s	[m ⁻¹]
Van Genuchten parameter	α	[-]
Van Genuchten parameter	β	[m ⁻¹]
Residual water saturation	S_{wr}	[-]
Coupling length	L_c	[m]
Manning roughness coefficient	n_x	[m ^{-1/3} s]
Manning roughness coefficient	n_y	[m ^{-1/3} s]
Evaporation depth	L_e	[m]
Evaporation limiting saturations	θ_{e1} θ_{e2}	[-]
Leaf Area Index	LAI	[-]
Root depth	L_r	[m]
Transpiration fitting parameters	C1, C2, C3	[-]
Transpiration limiting saturations	θ_{t1} θ_{t2}	[-]
Canopy storage parameter	C_{int}	[m]

852

853

854

855 **Table 2:** Calibrated saturated hydraulic conductivities and Van Genuchten parameters.

Units	K[m/s]	Residual water saturation	Van Genuchten parameters	
Continental Terminal	$1.12 \cdot 10^{-5}$	0.023	0.088	1.113
Weathered zone	$1.24 \cdot 10^{-6}$	0.042	0.166	1.128
Schistes	$6.36 \cdot 10^{-9}$	0.042	0.100	1.153
Granites	$9 \cdot 10^{-8}$	0.079	0.134	1.34

856

857 **Table 3:** Calibrated Transpiration and Overland flow parameters

Parameters	Agriculture	Savanna	Steppe	Urban	Bare soil
Max Leaf Area Index [-]	1.2	1.25	1.2	0.2	0.01
Root depth [m]	1.5	4.5	1	0.1	0.01
Manning friction Coefficients [m ^{-1/3} s]	0.139	0.187	0.154	0.016	0.43
Coupling Length [m]	0.01	0.01	0.01	0.1	0.01

858

859

860

861 **Table 4:** Water balance profiles for different land use types

Land Use	Infiltration (mm/year)	Total ET	Recharge	Groundwater Discharge
Fallow/ Agriculture	119	51	68	0
Sahelian Savanna	93	103	0	0
Pond type 1	203	101	203	213
Pond type 2	174	97	174	0
Niger River (loosing zone)	98	67	98	0
Niger River (Gaining zone)	138	112	0	138
Ephemeral Stream	70	49	70	0

862

863

864 **Table 5:** Basin Average water balance (5 Years)

Rainfall	Infiltration	Surface Evaporation	Overland Flow	Transpiration	Total ET	Recharge	Groundwater Discharge	Balance Error
580.88	92.4	139	63.4	247	386	28.6	9.66	0.82
100%	15.9	8.64	10.91	58.01	66.31	4.92	1.66	0.14

865

866

867

868

869

870

871

872

873

874

875

876

877 References

878

879 Amogu O, Descroix L, Yéro S Kadidiatou , Le Breton E , Mamadou I , Ali A, Vischel T,
 880 Bader J Claude , Moussa B Ibrahim , Gautier E , Boubkraoui S and Belleudy P (2010)
 881 Increasing River Flows in the Sahel? Water, ISSN 2073-4441

882

883 Andersson Jafet C.M., Ali Abdou , Arheimer Berit, Gustafsson David , Minoungou Bernard
 884 (2017) . Providing peak river flow statistics and forecasting in the Niger Riverbasin. Physics
 885 and Chemistry of the Earth 100 3- 12

886

887 Andersen, I., O. Dione, M. Jarosewich-Holder, and J. C. Olivry (2005). The Niger River
 888 basin: A vision for sustainable management, World Bank Publications. [Available at
 889 [http://siteresources.worldbank.org/INTWAT/Resources/4602114-1206643460526/
 890 Niger_River_Basin_Vision_Sustainable_Management.pdf](http://siteresources.worldbank.org/INTWAT/Resources/4602114-1206643460526/Niger_River_Basin_Vision_Sustainable_Management.pdf).

891

892

893 Aquanty Inc. (2017). HGS User Manual. Available
 894 at [https://static1.squarespace.com/static/54611cc8e4b0f88a2c1abc57/t/59cea33846
 895 c3c4384b8e5de1/1506714438873/hydrosphere_user.pdf](https://static1.squarespace.com/static/54611cc8e4b0f88a2c1abc57/t/59cea33846c3c4384b8e5de1/1506714438873/hydrosphere_user.pdf)

896

897

898 Barthel, R., and Banzhaf, S. (2016). Groundwater and surface water interaction at the
 899 regional-scale—a review with focus on regional integrated models. Water resources
 900 management, 30(1), 1-32

901 Berg, S.J. and Sudicky, E.A., 2019. Toward Large-Scale Integrated Surface and Subsurface
 902 Modeling. Groundwater, 57(1), pp.1-2.

903 Bernert G, Dehays H, Garin H, Zunino C (1985) Programme d'urgence pour le renforcement
 904 de l'alimentation en eau potable des quartiers périphériques de Niamey (Niger): exécution de
 905 50 forages productifs [Emergency program to strengthen the supply of drinking water in
 906 suburban areas of the city of Niamey (Niger): execution of 50 productive boreholes].
 907 Technical report BRGM/MHE, BRGM, Orléans, France, 52 pp

908

909 Boulain N, Cappelaere B, Ramier D, Issoufou HBA, Halilou O, Seghieri J, Guillemain F, Oï
 910 M, Gignoux J, Timouk F (2009) Towards an understanding of coupled physical and
 911 biological processes in the cultivated Sahel: 2. vegetation and carbon dynamics. J Hydrol
 912 375:190-203

913

914

915 Brooks, R.H., Corey, A.T., (1964) . Hydraulic properties of porous media and their relation to
 916 drainage design. Trans. ASAE 7 (1), 26-0028

917

- 918 Chardon D., Grimaud J-L., Beauvais A. and Bamba O. (2018). West African lateritic
919 pediments: Landform-regolith evolution processes and mineral exploration pitfalls. Elsevier,
920 Earth-Science Reviews, 124–146p
921
- 922 Chen, J., E.A. Sudicky, J.H. Davison, S.K. Frey, Y. -J. Park, H. -T. Hwang, A.R. Erler, S.J.
923 Berg, M.V. Callaghan, K. Miller, M. Ross, W.R. Peltier. Towards a Climate-Driven
924 Simulation of Coupled Surface-Subsurface Hydrology at the Continental Scale: A Canadian
925 Example. Canadian Water Resources Journal: Under Review
926
927
928
- 929 CILSS (2016) Landscapes of West Africa – A Window on a Changing World. U.S.
930 Geological Survey EROS, 47914 252nd St, Garretson, SD 57030, UNITED STATES
- 931
- 932 Dai Aiguo., Lamb J Peter., Trenberth E Kevin., Hulme Mike., Jones D Philip., And Xie
933 Pingping (2004). Comment The recent Sahel drought is real. Int. J. Climatol. 24: 1323-
934 1331
935
936
- 937 Dehays H, Garin H, Zunino C (1986) Programme d’urgence pour le renforcement de
938 l’alimentation en eau potable des quartiers périphériques de Niamey (Niger): deuxième
939 phase—exécution de 68 forages [Emergency program to strengthen drinking water supply in
940 suburban areas of the city of Niamey (Niger): second phase— execution of 68 boreholes].
941 Technical report BRGM/MHE, BRGM, Orléans, France, 30 pp
942
943
944
945
- 946 Desconnets JC, Taupin JD, Lebel T, Leduc C (1997). Hydrology of the Hapex-Sahel Central
947 Super-Site: surface water drainage and aquifer recharge through the pool systems. J Hydrol
948 188–189:155–178
949
950
- 951 Erler, A. R., Frey, S. K., Khader, O., d’Orgeville, M., Park, Y.-J., Hwang, H.-T., et al. (2019).
952 Simulating climate change impacts on surface water resources within a lake-affected region
953 using regional climate projections. Water Resources Research, 55, 130–155. [https://](https://doi.org/10.1029/2018WR024381)
954 doi.org/10.1029/2018WR024381
- 955
- 956 Favreau G, Cappelaere B, Massuel S, Leblanc M, Boucher M, Boulain N, Leduc C (2009) Land
957 clearing, climate variability and water resources increase in semiarid southwest Niger: a
958 review. Water Resour Res 45:W00A16
959
- 960 Favreau G (2000) Caractérisation et modélisation d’une nappe phréatique en hausse au Sahel:
961 dynamique et géochimie de la dépression piézométrique naturelle du kori de Dantiandou (sud-
962 ouest du Niger) [Characterization and modelling of a rising water table in the Sahel: dynamics

- 963 and geochemistry of the Dantiandou kori natural piezometric depression (southwest Niger)].
964 PhD Thesis, Univ Paris XI, Orsay, France, 258 pp
965
- 966 Favreau, G.,(1996). Modélisation locale de la recharge de la nappe phréatique sur le site de
967 Wankama (sud-ouest du Niger). Mémoire de 3^e cycle universitaire (DEA), 75 p. Université
968 de Paris-sud / Orsay, France.
969
- 970 Favreau, G., Leduc, C.,(1998). Fluctuations à long terme de la nappe phréatique du
971 Continental Terminal près de Niamey (Niger) entre 1956 et 1997. in : “Variabilité des
972 ressources en eau en Afrique au XX^eme siècle”, conférence Abidjan’98, 1998. AISHPubl.,
973 252,253-2588.
974
- 975 Girard P (1993) Techniques isotopiques (¹⁵N, ¹⁸O) appliquées à l’étude des nappes des
976 altérites et du socle fracturé de l’Ouest Africain: l’Ouest du Niger [Isotopic techniques
977 applied to groundwaters of alterites and fractured basement aquifers in West Africa:
978 the Western Niger]. PhD Thesis, Univ of Quebec at Montreal, Canada, 141 pp
979
- 980 Girard P, Hillaire-Marcel C, Oga MS (1997) Determining the recharge mode of Sahelian
981 aquifers using water isotopes. *J Hydrol* 197:189– 202
982
- 983 Goderniaux, P., Brouyère, S., Fowler, H. J., Blenkinsop, S., Therrien, R., Orban, P., &
984 Dassargues, A. (2009). Large scale surface–subsurface hydrological model to assess
985 climate change impacts on groundwater reserves. *Journal of Hydrology*, 373(1-2),
986 122-138
987
- 988
- 989 Hassane, Aïssata B., Christian, L. ., Favreau, G., Barbara,A. B., Thomas, M (2016) . Impacts
990 of a large Sahelian city on groundwater hydrodynamics and quality: example of Niamey
991 (Niger). *Hydrogeology Journal*,
992
- 993 Hornberger, M.G., Raffensperger, J.P., Wilberg, P.L., Eshleman, K.L., 1998. Elements of
994 Physical Hydrology. JUH Press. 312 pp.
995
- 996
- 997 Hwang, H.T., Park, Y.J., Sudicky, E.A., Berg, S.J., McLaughlin, R. and Jones, J.P.,2018.
998 Understanding the water balance paradox in the Athabasca River Basin,
999 Canada. *Hydrological processes*, 32(6), pp.729-746.
1000
- 1001 Hwang, H.T., Park, Y.J., Frey, S.K., Berg, S.J. and Sudicky, E.A., 2015. A simple iterative
1002 method for estimating evapotranspiration with integrated surface/subsurface flow
1003 models. *Journal of Hydrology*, 531, pp.949-959.
1004
- 1005 Hwang, H. T., Y. J. Park, E. A. Sudicky, P. A. Forsyth (2014) A parallel computational
1006 framework to solve flow and transport in integrated surface–subsurface hydrologic
1007 systems, *Environ Model Software*, 61 (0), 39-58.
1008
1009

- 1010 Ibrahim. M., Favreau.G., Scanlon, R.B ., Luc,S.J., Le Coz, M., Demarty. J., Cappelaere.B
 1011 (2014) . Long-term increase in diffuse groundwater recharge following expansion of rainfed
 1012 cultivation in the Sahel, West Africa 1293-1305 Hydrogeology Journal
 1013
- 1014 Jones, J.-P., (2005). Simulating hydrologic systems using a physically-based surface
 1015 subsurface model: issues concerning flow, transport and parameterization. Ph.D. Thesis,
 1016 University of Waterloo, Waterloo (Canada), 145 pp.
 1017
- 1018 Kristensen, K.J., Jensen, S.E., (1975). A model for estimating actual evapotranspiration from
 1019 potential evapotranspiration. Nordic Hydrology 6, 170–188.
 1020
- 1021 Lebel, T; Ali, A.,(2007). Recent trends in the Central and Western Sahel rainfall regime
 1022 (1990–2007) Journal of Hydrology 375 52–64
 1023
- 1024 Lebel .T, Taupin .J.D, D’Amato .N . (1997) . Rainfall monitoring during HAPEX-Sahel. 1.
 1025 General rainfall conditions and climatology. Journal of Hydrology 74-96
- 1026 Leduc C, Favreau G, Schroeter P (2001) Long-term rise in a Sahelian water-table: the
 1027 Continental Terminal in south-west Niger. J Hydrol 243:43–54
 1028
- 1029 Levy P.E., Jarvis P.G. (1997). Direct and indirect measurements of LAI in millet and fallow
 1030 vegetation in HAPEX-Sahel . Agricultural and Forest Meteorology 97 199–212
 1031
- 1032 Li, Q., Unger, A.J.A., Sudicky, E.A., Kassenaar, D., Wexler, E.J., Shikaze, S., (2008)
 1033 .Simulating the multi-seasonal response of a large-scale watershed with a 3D physically-based
 1034 hydrologic model. Journal of Hydrology 357 (3–4), 317–336.
 1035
- 1036 Luigi P., Giovanna, A.D., Manuela. L., Konaté.M., Francesco.S, Guero. Y., A., Tankari,D.B.,
 1037 Domenico.A.De.L (2016). Monitoring of urban growth and its related environmental impacts:
 1038 Niamey case study (Niger). *Energy Procedia*, 97 (2016) 37 – 43.
 1039
- 1040 Machens E. (1973). Contribution à l’étude des formations du socle cristallin et de la
 1041 couverture sédimentaire de l’Ouest de la République du Niger, 3 Mém. BRGM, Fr.,1973, n°
 1042 82, 167 pages.
 1043
- 1044
- 1045 Mahé, G., F. Bamba, A. Soumaguel, D. Orange, and J. C. Olivry (2009), Water losses in the
 1046 inner delta of the River Niger: Water balance and flooded area, Hydrol. Process., 23, 3157–
 1047 3160.
 1048
- 1049 Mascaro, G., D. D. White, P. Westerhoff, and N. Bliss (2015), Performance of the CORDEX-
 1050 Africa regional climate simulations in representing the hydrological cycle of the Niger River
 1051 basin, J. Geophys. Res. Atmos., 120,12,425–12,444, doi:10.1002/ 2015JD023905

1052

1053 Mamadou I., Gautier E., Descroix L., Noma I., Bouzou Moussa I., Faran Maiga O., Genthon
1054 P., Amogu O., Malam Abdou M., Vandervaere J.P., (2015). Exorheism growth as an
1055 explanation of increasing flooding in the Sahel. *Catena* 131, 130-139.

1056

1057 Massuel S, Cappelaere B, Favreau G, Lebel T, Vischel T (2011) Integrated surface water-
1058 groundwater modelling in the context of increasing water reserves of a regional Sahelian
1059 aquifer. *Hydrol Sci J* 56:1242–1264

1060

1061 Moeck C, Hunkeler D, and Brunner P (2015). Tutorials as a flexible alternative to GUIs: An
1062 example for advanced model calibration using Pilot Points. *Environmental Modelling &*
1063 *Software* 66-78e86

1064

1065 Ramier D, Boulain N, Cappelaere B, Timouk F, Rabanit M, Lloyd CR, Boubkraoui S,
1066 Metayer F, Descroix L, Wawrzyniak V (2009) Towards an understanding of coupled physical
1067 and biological processes in the cultivated Sahel: 1. energy and water. *J Hydrol* 375:204-216

1068

1069

1070 Rockstrom J, Jansson PE, Barron J (1998) Seasonal rainfall partitioning under runoff and
1071 runoff conditions on sandy soil in Niger: on-farm measurements and water balance modeling.
1072 *J Hydrol* 210:68-92

1073

1074 Schaap, M.G., F.J. Leij, and M.T. Van Genuchten. (2001). ROSETTA: A computer program
1075 for estimating soil hydraulic parameters with hierarchical pedotransfer functions. *Journal of*
1076 *Hydrology* 251, no. 3: 163–176.

1077

1078 Soumaïla A. et Konaté M. (2005). Caractérisation de la déformation dans la ceinture
1079 birimienne (paléoprotérozoïque) de Diagorou-Darbani (Liptako nigérien, Afrique de l'Ouest).
1080 *Africa Geoscience Review*, 2005, Vol. 12, No. 3, pp. 161-178.

1081

1082 Sudicky, E.A., Jones, J.-P., Park, Y.-J., Brookfield, E.A., Colautti, D., (2008). Simulating
1083 complex flow and transport dynamics in an integrated surface-subsurface modeling
1084 framework. *Geosciences Journal* 12 (2), 107–122.

1085

1086

1087

1088 Tarhule A and Lamb J. P (2003). Climate Research and Seasonal Forecasting for West
1089 Africans: Perceptions, Dissemination, and Use?: Perceptions, Dissemination, and Use? .

1090

1091

1092

1093 Therrien, R., McLaren, R.G., Sudicky, E.A., Panday, S.M., 2005. HydroGeoSphere. A three-
1094 dimensional numerical model describing fully-integrated subsurface and surface flow and
1095 solute transport, 5, 343 pp

1096

1097 Van Genuchten, M.Th., (1980). A closed-form equation equation for predicting the hydraulic
1098 conductivity of unsaturated soils, Soil Sci. Soc. Am. J., 44, 892{898.

1099
1100
1101
1102
1103
1104
1105
1106
1107
1108
1109
1110
1111
1112
1113
1114
1115
1116
1117
1118
1119
1120
1121
1122
1123
1124
1125
1126
1127
1128
1129
1130
1131
1132
1133
1134
1135
1136
1137
1138
1139
1140
1141
1142
1143
1144
1145
1146

Journal Pre-proof

1147 **Declarations of interest: none.**

1148

1149

1150

1151

1152

1153

1154

1155 **Acknowledgements**

1156

1157 This work was supported by the German Federal Ministry of Education and Research
1158 (BMBF) under Grant No. 01LG1202E of the WASCAL project.

1159 This work was supported by Aquanty's Visiting Student Program.

1160

1161

1162

1163

1164

1165

1166

Journal Pre-proof

Characterization of groundwater –surface water interactions using high resolution integrated 3D hydrological model in semiarid urban watershed of Niamey, Niger.

Abdou Boko Boubacar^{1, 2}, Konaté Moussa², Nicaise Yalo³, Steven J. Berg^{4, 5}, Andre R. Erler^{4, 6}, Hyoun-Tae Hwang^{4, 5}, Omar Khader⁴, Edward A. Sudicky^{4, 5}

Highlights:

- A methodological framework for integrated hydrological model calibration in a data scarce watershed is described
- The Niger river acts as a natural groundwater discharge zone
- Intense rainfall has significant impact on river aquifer exchange fluxes
- Plant transpiration dominates the water balance.

Keywords: Groundwater –Surface water interactions, calibration, integrated hydrological model, semi arid.

Declarations of interest:

The authors declare that they have no known competing financial interests or personal relationships that could have appeared to influence the work reported in this paper.

Journal Pre-proof